Local atomic ordering and nanoscale phase separation in a Pd-Ni-P bulk metallic glass

Yoshihiko Hirotsu,[1,*] T. G. Nieh,[2] Akihiko Hirata,[1] Tadakatsu Ohkubo,[3] and Nobuo Tanaka[4]
[1]*The Institute of Scientific and Industrial Research, Osaka University, 8-1 Mihogaoka, Ibaraki, Osaka 567-0047, Japan*
[2]*Department of Materials Science and Engineering, The University of Tennessee, Knoxville, Tennessee 37996-2200, USA*
[3]*National Institute for Materials Science, 1-2-1 Sengen, Tsukuba 305-0047, Japan*
[4]*Ecotopia Research Institute and Department of Crystalline Materials Science, Nagoya University, Chikusa-ku, Nagoya, 464-0846, Japan*
(Received 15 July 2005; revised manuscript received 3 October 2005; published 24 January 2006)

The local structure in a $Pd_{40}Ni_{40}P_{20}$ bulk metallic glass was examined using a spherical-aberration-corrected high resolution TEM. Fcc-Pd(Ni) type nanoclusters and local compound (phosphide)-like nanoclusters with sizes of 1–2 nm embedded in a dense-randomly-packed amorphous matrix were clearly observed under an appropriate imaging condition. However, three-dimensional atom-probe elemental mapping revealed there is virtually no nanoscale compositional difference between the nanoclusters and amorphous matrix beyond the statistical error range. A very small interfacial energy between the nanophase and the matrix is able to form a metastable amorphous phase with a structural fluctuation.

DOI: 10.1103/PhysRevB.73.012205 PACS number(s): 81.05.Kf, 61.43.Dq, 68.37.Lp

Some metallic glass systems to form bulk metallic glasses have been found in recent years.[1,2] Atomic arrangements of metallic glasses have been attracting much interest especially for glasses with a large glass forming ability in order to find the structural reason for the good glass forming alloys. Since metallic glasses are generally formed using eutectic alloy systems (especially with deep eutectic temperatures), local structural and compositional fluctuations are considered to occur during their glass forming process of cooling when metal atom diffusion is not interrupted during cooling. Such local fluctuations presumably accompany the local atomic order beyond the nearest neighbor distances [called medium range order (MRO)], and are correlated with the nanoscale phase separation (decomposition). The bulk form of $Pd_{40}Ni_{40}P_{20}$ glass was first obtained by Drehman *et al.*[3] Subsequently, scanning calorimetry[4] and TEM studies[5,6] were performed on the annealing stage of this alloy with P compositions less than 19 at. %, and amorphous phase separation and PdNi fcc nanocrystal formation on annealing were discussed.[3,6] No study has since been done to know details of the local structures not only of the annealed state, but also of the as formed state of the bulk Pd-Ni-P glasses. Using high resolution electron microscopy (HREM) and nanobeam electron diffraction, the present authors have observed glass structures with nanoscale phase separation in Pd-Si (Ref. 7) and Fe-Nb-B (Ref. 8) glasses through local structural fluctuations. In this sense, MRO structures or nanoscale local structures with structural and compositional fluctuations in this bulk metallic Pd-Ni-P glass warrant a thorough investigation using HREM.

Attempts to directly observe metallic glass local structures by the HREM especially to image the MRO structures began in the late 1970s.[9] It was then realized that a sharp atomic image of local structures by this technique was not possible, mainly because a strong background noise arising from an electron optical function produced by spherical aberration of objective lens and defocus. This electron optical function ruling over a phase change in the phase contrast imaging is known as "phase contrast transfer function" (PCTF).[10,11] For imaging of local crystalline nanoclusters in amorphous alloys, experimental efforts to minimize the background noise caused by the PCTF have only limited success.[12–15] As a result, the morphologies of these nanoclusters, such as size distribution and degree of lattice distortion, could not be accurately measured. In addition, chemical compositions of these local structures were difficult to determine because of the lack of the proper analytical tool.

Recent advances of the HREM, especially with the availability of spherical-aberration-corrected (C_S corrected) atomic imaging, made it possible to directly observe local structures in the atomic scale. C_S corrected atomic imaging has now been developed for both conventional type[16] and scanning transmission type[17] TEMs. For instance, subangstrom atomic imaging,[18] local crystallinity of amorphous Si,[19] interfacial structure of SiO_2/Si,[20] and atomic arrangements in semiconductors[21,22] have been demonstrated using the C_S corrected TEM. In order to clarify, primarily, size distribution and lattice distortion of the nanoclusters, thus, we used a C_S corrected TEM (200 kV) to directly observe local atomic structure in a $Pd_{40}Ni_{40}P_{20}$ glass in the present study.

Prior to using C_S corrected TEM, local structures of the $Pd_{40}Ni_{40}P_{20}$ were initially examined using a conventional high-resolution TEM (JEM-3000F, 300 kV, C_S=0.6 mm). A bulk amorphous $Pd_{40}Ni_{40}P_{20}$ sample with a diameter of 5 mm and 50 mm long was fabricated by a Cu mold casting method. The amorphous structure was confirmed by x-ray diffraction. For the TEM observations, a thin slice of the cast rod was mechanically thinned down to about 20 μm in flowing water, followed by a conventional ion thinning. Despite the fact that selected area electron diffraction shows a typical halo pattern, local lattice fringes extending to ~2 nm can be readily seen in the specimen. HREM images from two adjacent areas are shown in Figs. 1(a) and 1(b), which were taken near the optimum defocus condition of $\Delta f \sim 110$ nm (underfocus). Such local lattice images as seen in Fig. 1 were also observed in a specimen prepared by electrolytic thinning. In Fig. 1, fcc-Pd type clusters with the [100] and [110] orientations are indicated in regions *A* and *B*, respectively. From the fringe spacings and fringe intersecting angles, these regions can be identified as fcc-Pd type clusters.[7,14] However, although these fcc clusters are identifiable, quantitative infor-

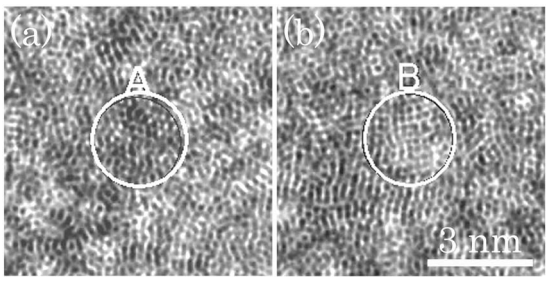

FIG. 1. High resolution TEM image of $Pd_{40}Cu_{40}P_{20}$ BMG taken by a conventional TEM (C_S=0.6 mm) at Δf~110 nm. Crossed lattice fringe regions resembling [110] and [100] oriented fcc-Pd(Ni,P) clusters can be seen at *A* and *B*, respectively.

mation such as the exact size and the degree of distortion cannot be accurately measured because of a high background image noise.

Before using C_S corrected TEM (200 kV), we further calculated through focus axial beam HREM images for a structure model under different Cs values in order to find the optimum Cs and defocusing conditions for clear imaging. We constructed a structure model based on the observation of the fcc type clusters (Fig. 1) in which four fcc clusters (with Pd and Ni at the fcc lattice sites, and P at both the substitutional and interstitial sites) were inserted into a DRP matrix consisting of Pd, Ni, and P atoms. The composition of the clusters was fixed at $Pd_{40}Ni_{40}P_{20}$, the same as that of the DRP matrix. The model structure is a tetragonal cell with dimensions of 4.2 nm$\times$4.2 nm$\times$5.0 nm. In this cell, two fcc clusters with a diameter of 2 nm are [110] and [100] orientated, and another two are [110] orientated but with different diameters of 1.5 and 1.0 nm. All the fcc clusters were placed at the middle distance of cell along the tetragonal long axis (defined here as *c* axis). The total number of atoms in the tetragonal cell was 6221 determined after the measurement of physical density of the specimen (9.4 g/cm^3). The model structure viewed along the *c* axis (beam direction) is schematically illustrated in Fig. 2(a). The DRP matrix structure was initially constructed using a molecular dynamics technique under a periodic boundary condition, followed by replacing DRP regions with the four clusters. After the replacement, DRP atoms in the vicinity of these fcc clusters were relaxed using Lennard-Jones type atomic potentials. For image simulations, the direction of observation (i.e., beam direction) was chosen to be along the *c* axis. The multislice calculation technique with a fast Fourier transform[23] (FFT) was used, which included, in the present case, an aberration function with the third and fifth order spherical aberration constants, C_{S3} and C_{S5}, respectively.[24] The value of C_{S3} (generally assigned as Cs) is variable by the Cs corrector, and the value of C_{S5} was taken as 5 mm according to the design of the objective and C_S corrector lenses of the present C_S corrector.[25] The envelope function due to beam convergence[26] and chromatic aberration[27] was also taken into consideration (beam divergence: 1×10^{-3} rad; energy spread transferred to defocus: 6 nm). According to the simulations it was concluded that the quality of local lattice images from the fcc clusters is significantly improved when $C_S \leqslant 20$ μm, especially at a small Δf value. In Figs. 2(b)–2(d), a set of

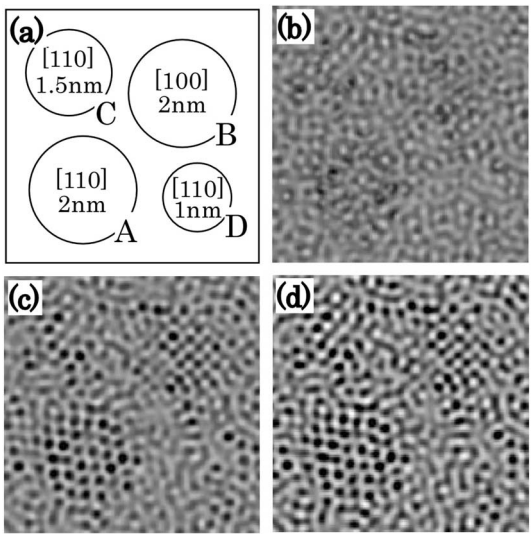

FIG. 2. (a) Structure model (schematic) of $Pd_{40}Cu_{40}P_{20}$ with fcc-Pd(Ni,P) clusters embedded in a DRP matrix viewed along the beam direction. Structure size: 4.2 nm$\times$4.2 nm$\times$5.0 nm. The beam direction: along the thickness of 5.0 nm. Cluster sizes: 2 nm for *A* and *B* clusters, 1.5 nm for *C* and 1 nm for *D*. Cluster orientations: [110] for *B*, *C*, and *D*, and [100] for *A*. (b)–(d) Simulated through-focus images of the C_S corrected TEM for the structure in (a) for C_S=2 μm. Defocus values are: (b) 0 nm, (c) 5 nm, and (d) 9 nm (underfocus).

simulated HREM images for the structure model is shown which were calculated under the C_S value of 2 μm and under the defocus values of 0, 5, and 9 nm (underfocus). It is noted that under the defocus Δf=0 nm, we have almost no contrast of the fcc cluster images. On the other hand, under Δf =5 nm, images (dark dots represent Pd atoms) at regions *A* and *B* are so sharp that the cluster size as well as shapes can be irrevocably identified. At a higher Δf value (e.g., $\Delta f \gtrsim 9$ nm), however, the background noise intensifies and the boundary between the cluster and the matrix became blurry. From the simulated images it is particularly noted that, although embedded 2 nm crystalline clusters can be sharply imaged under appropriate imaging conditions, it is extremely difficult to capture the lattice images of clusters smaller than 1 nm. For instance, lattice image of the [110] oriented 1 nm fcc cluster [region *D* in Fig. 2(a)] is not discernible unless at Δf=5 nm and C_S=2 μm. Simulated images at C_S=0 or less (e.g., C_S=−2,−12 μm) are essentially almost the same as those obtained at C_S=2 μm.

To conduct structure observation, a C_S corrected TEM, JEM-2010FC operated at 200 kV, was used. In the specimen preparation especially for the Cs corrected TEM study, the ion milling was initially performed using PIPS (Gatan model) with a voltage of 2 kV and at a low glancing angle of 3°, followed by a final thinning at a low voltage of at 200 V and a glancing angle of 10° (Techno-Linda model).

We performed a through-focus imaging of the structure of the present Pd-Ni-P by using the same C_S value of 2 μm. Images taken at Δf values of 1, 5, and 9 nm (underfocus) are shown in Figs. 3(a)–3(c), respectively. Atomic image contrasts of crystalline cluster as a function of Δf are noted to agree remarkably well with those from simulations. Specifi-

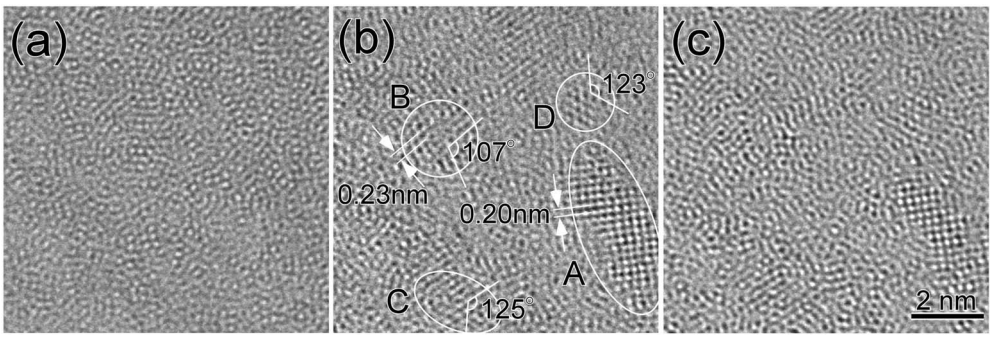

FIG. 3. High-resolution images taken by a C_S corrected TEM at C_S=2 μm and $\Delta f \sim 1$ nm (a), 5 nm (b), and 9 nm (c).

cally, at $\Delta f \sim 0-1$ nm the image contrast is low and no cluster is revealed, but at $\Delta f = 5$ nm, extended local clusters are clearly observed with dark spots representing atomic positions in the encircled regions in Fig. 3(b). At an increasing Δf value of 9 nm, images of these clusters gradually shrink as the background contrast increases. From the spacings and intersecting angles of the lattice fringes, images at *A* and *B* in Fig. 3(b) are readily identified as [100]- and [110]-oriented fcc-Pd-type clusters. Whereas cluster *B* appears to be spherical, cluster *A* is ellipsoidal, suggesting there exists a structural anisotropy. The average lattice parameter of cluster *A* was determined to be 0.411 nm from the fringe spacings (for calibration, we used lattice images of Au particles as standard). This value is larger than the lattice parameters for both fcc-Pd (0.389 nm) and fcc-Ni (0.352 nm). Atomic radii of Pd, Ni, and P, are 0.137, 0.124, and 0.106 nm, respectively, which are relatively close to one another. Pd and Ni form a complete solid solution. Additional P can occupy either substitutional or interstitial sites. From the observed lattice parameter of the cluster, it is conceivable that the fcc clusters contain significant amount of P atoms at the interstices. The clusters can thus be denoted as fcc-Pd (Ni,P) or fcc-(Pd,Ni,P). The lattice image geometries of clusters *C* and *D* are somewhat similar to those [110] lattice image of fcc-Pd(Ni,P), having similar lattice fringe spacings. However, in each of these images the angle between the two sets of lattice fringes differs by about 15° from that of the [110] fcc-Pd(Ni,P) image (cf. cross angles for clusters *B*, *C*, and *D*). The lattice images in *C* and *D* are, in fact, quite similar to the image of $[1\bar{2}4]$ Ni_2P. From these sharp local nanosized crystalline cluster images it was concluded that a "nanoscale phase separation" with the formation of fcc-Pd(Ni,P) and phosphide nanophases takes place during cooling of Pd-Ni-P melt. It should be noted that in the HREM the crystalline cluster regions with sizes larger than 2 nm were not frequently observed, but in most cases the cluster sizes were as small as 1 nm as seen in Fig. 3(b) as clusters *B*, *C*, and *D*.

Although we can nicely identify the structure of nanoclusters in the Pd-Ni-P metallic glass using a C_s corrected HREM, the C_s corrected HREM cannot provide the chemical information of the nanoclusters. To obtain the chemical composition of these fcc nanoclusters we further carried out atom probe (AP) elemental mapping analysis using a 3D AP equipped with a tomographic atom probe detection system (CAMECA). The specimen for AP imaging was prepared by electrolytic thinning. A 3D AP elemental mapping was performed for Pd, Ni, and P distributed in a cell of 40 nm $\times$ 10 nm $\times$ 9 nm in the *as* formed specimen. The chemical composition measured by the 3D AP was $Pd_{40}Ni_{37}P_{23}$, and is almost equal to the nominal composition of the specimen. It was found that Pd, Ni, and P atoms are distributed rather uniformly in the entire cell. Figure 4 shows a set of 3D AP compositional profiles taken from a small cell (2 nm $\times$ 2 nm $\times$ 40 nm). It is evident that there is no clear compositional modulation even in the nanoscale, nor clear correlations between the compositional changes for Pd, Ni, and P atoms are observed in the figure. Although nanometer sized clusters (or MROs) are embedded in the amorphous matrix, their chemical compositions appear to be essentially the same as the composition of the matrix. However, we cannot exclude the possibility of having a small local compositional variation because of the large statistical errors in the 3D AP imaging when the examining area is at nanosize. It is conceivable that atom distribution in the liquid state was initially random. During cooling, short range atomic diffusion, as small as one to two atomic distance, can still take place to

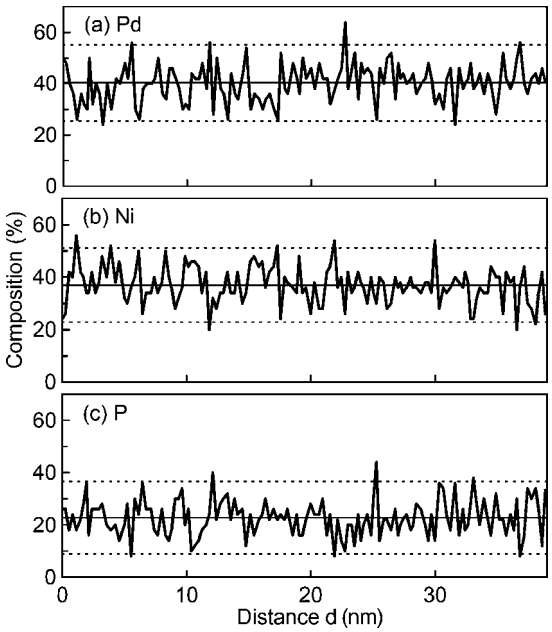

FIG. 4. Compositional changes of Pd(a), Ni(b), and P(c) within a area of 2 nm $\times$ 2 nm $\times$ 40 nm in the $Pd_{40}Cu_{40}P_{20}$ bulk metallic glass. The compositional profiles were taken from the 3D AP elemental map with a cell size of 9 nm $\times$ 10 nm $\times$ 40 nm. In the figures (a), (b), and (c) dotted-lines correspond to statistical error ranges (2σ).

minimize the local free energy. This atomic rearrangement can cause a small local compositional fluctuation, but it is within the detection error of the 3D AP. Also, this small local compositional fluctuation can trigger the subsequent local structural variation and result in the nanoscale phase separation. Since an appreciable compositional variation is negligible, the interfacial energy between the nanoclusters and the matrix is very small; this stabilizes the metastable amorphous phase with a structural fluctuation.

As suggested by the 3D-AP study, there is no clear compositional variation throughout the specimen. This means that the atomic composition distribution is almost the same as that in the liquid state, and no local primary phase nucleation and growth was occurring during quenching. Supposing that the fcc nanoclusters observed are all potentially nuclei, the final number density of the primary phase (fcc-Pd) must be as large as $10^{25}/m^3$ or more, which is 14 order of magnitude larger than the real number density.[28] From the above considerations most of the presently observed fcc-Pd type nanoclusters in the amorphous Pd-Ni-P structure cannot be taken as quenched in nuclei of the primary phase in crystallization. After the classical nucleation and growth theory, most of the observed local ordered regions can be called "crystal embryos."[29] fcc nanoclusters larger than 2 or 3 nm (with less observation chances) may have a possibility to be taken as quenched in nuclei, but we have no evidence at this moment. We need a further detailed experimental study to know a role of the nanoclusters on the primary crystallization process using a HREM observation, together with a theoretical study for the correct estimation of the critical size.

As discussed before, a large lattice distortion exists in some nanoclusters [Fig. 3(b)]. The distortion is mainly caused by the substitution of large Pd atoms with smaller P atoms, or the insertion of P atoms into interstitial sites. The heavily deformed crystalline clusters are accompanied by a diffuse structural interface between the clusters and the amorphous matrix. This is why diffraction from a glass structure containing such nanoclusters often exhibits a typical halo pattern.[15]

In summary, we used a high resolution TEM attached with a C_S corrector for aberration correction to examine MRO structures in a $Pd_{40}Ni_{40}P_{20}$ bulk metallic glass. We demonstrated that, when the spherical aberration constant was close to zero and the defocus value was near the Gaussian focus, sharp lattice images of crystalline nanoclusters with a size of $\sim 1-2$ nm can be clearly identified. These nanoclusters identified are with an fcc-Pd type structure, and also with a compound (phosphide) structure. These nanoclusters are largely distorted because of the possible inclusion of a significant amount of P atoms. 3D AP analysis in the present study did not show an appreciable compositional variation in space in the as-formed state, suggesting "nanoscale phase separation" in the present material does not necessary accompany an appreciable amount of compositional fluctuation. It is possible that the nm sized structural modulation initially observed by the TEM near Tg in the annealed Pd-Ni-P glass[6] corresponds to the development of the present type of nanoscale phase decomposed structure. The estimated density of the nanoclusters was found extremely high. The role of these nanoclusters on the subsequent crystallization behavior of the alloy is yet to be studied.

The authors thank Drs. H. Sawada and T. Oikawa of JEOL Ltd for helping the HREM study with the C_S corrector. The authors also thank Dr. K. Hono, Dr. J. Wang, Dr. J. Yamasaki, and Dr. T. Hanada for their help and valuable discussions. This work is partly supported by the Grant in Aid of Ministry of Education, Sports, Culture, Science, and Technology, Priority Area on "Materials Science of Bulk Metallic Glasses," and partly supported by the Division of Materials Sciences and Engineering, Office of Basic Energy Sciences, U.S. Department of Energy under Contract No. DE-AC05-00OR-22725 with UT-Battelle.

*Author to whom correspondence should be addressed. Electronic address: yhirotsu@sanken.osaka-u.ac.jp

[1] A. Inoue, Acta Mater. **48**, 279 (2000).
[2] A. Peker and W. L. Johnson, Appl. Phys. Lett. **63**, 2342 (1993).
[3] A. J. Drehman *et al.*, Appl. Phys. Lett. **41**, 716 (1982).
[4] H. S. Chen, Mater. Sci. Eng. **23**, 151 (1976).
[5] P. G. Boswell, Scr. Metall. **11**, 701 (1977).
[6] A. R. Yavari *et al.*, Scr. Metall. **22**, 1231 (1988).
[7] T. Ohkubo and Y. Hirotsu, Phys. Rev. B **67**, 094201-1 (2003).
[8] Y. Hirotsu *et al.*, Intermetallics **12**, 1081 (2004).
[9] W. M. Stobbs and D. J. Smith, Nature (London) **281**, 54 (1979).
[10] J. M. Cowley, *Diffraction Physics* (North-Holland, Amsterdam, 1981), Chap. 13.
[11] *High-Resolution Transmission Electron Microscopy and Associated Techniques*, edited by P. Busek *et al.* (Oxford Sci. Pub., New York, 1992), Chaps. 1 and 12.
[12] Y. Hirotsu and R. Akada, Jpn. J. Appl. Phys. **23**, L478 (1984).
[13] Y. Hirotsu *et al.*, J. Appl. Phys. **59**, 3081 (1986).
[14] K. Anazawa *et al.*, Acta Metall. Mater. **42**, 1997 (1996).
[15] Y. Hirotsu *et al.*, Microsc. Res. Tech. **40**, 284 (1998).
[16] M. Haider *et al.*, J. Electron Microsc. **47**, 395 (1998).
[17] O. L. Krivanek *et al.*, Ultramicroscopy **78**, 1 (1999).
[18] P. E. Batson *et al.*, Nature (London) **418**, 617 (2002).
[19] C. R. Perrey *et al.*, J. Non-Cryst. Solids **343**, 78 (2004).
[20] N. Tanaka *et al.*, J. Electron Microsc. **52**, 69 (2003).
[21] F. Hosokawa *et al.*, J. Electron Microsc. **52**, 3 (2003).
[22] L. Y. Chang *et al.*, J. Electron Microsc. **52**, 359 (2003).
[23] K. Ishizuka and N. Uyeda, Acta Crystallogr., Sect. A: Cryst. Phys., Diffr., Theor. Gen. Crystallogr. **A33**, 740 (1977).
[24] T. Hanai *et al.*, J. Electron Microsc. **33**, 329 (1984).
[25] JEOL Ltd. (private communication).
[26] X. Frank, Optik (Stuttgart) **38**, 519 (1973).
[27] P. L. Fejes, Acta Crystallogr., Sect. A: Cryst. Phys., Diffr., Theor. Gen. Crystallogr. **A33**, 109 (1977).
[28] A. J. Drehman and A. L. Greer, Acta Metall. **32**, 323 (1984).
[29] T. Hamada and F. E. Fujita, *Proceedings of Rapidly Qurenched Metals IV, 1981*, edited by T. Masumoto and K. Suzuki; Jpn. J. Appl. Phys., Part 1 **21**, 981 (1982).